AGU PUBLICATIONS

Geophysical Research Letters

RESEARCH LETTER
10.1002/2017GL076335

Key Points:
- The interannual relationship between the edge of the Hadley cell and subtropical dry zones varies greatly in models
- The relative magnitudes of the climate change-induced shifts of these metrics are also highly uncertain
- Differences in models' internal variability explain much of these differences in future projections

Supporting Information:
- Supporting Information S1

Correspondence to:
W. J. M. Seviour,
wseviou1@jhu.edu

Citation:
Seviour, W. J. M., Davis, S. M., Grise, K. M., & Waugh, D. W. (2018). Large uncertainty in the relative rates of dynamical and hydrological tropical expansion. *Geophysical Research Letters*, *45*, 1106–1113. https://doi.org/10.1002/2017GL076335

Received 7 NOV 2017
Accepted 27 DEC 2017
Accepted article online 3 JAN 2018
Published online 19 JAN 2018

Large Uncertainty in the Relative Rates of Dynamical and Hydrological Tropical Expansion

William J. M. Seviour[1], Sean M. Davis[2,3], Kevin M. Grise[4], and Darryn W. Waugh[1]

[1]Department of Earth and Planetary Sciences, The Johns Hopkins University, Baltimore, MD, USA, [2]NOAA Earth System Research Laboratory, Boulder, CO, USA, [3]Cooperative Institute for Research in Environmental Sciences (CIRES), University of Colorado Boulder, Boulder, CO, USA, [4]Department of Environmental Sciences, University of Virginia, Charlottesville, VA, USA

Abstract Climate models predict that the Hadley circulation will expand poleward in a warmer climate, a trend which may cause significant changes in global precipitation patterns. However, recent studies have disagreed as to how strongly changes in the Hadley circulation and changes in the hydrological cycle (specifically the latitude at which precipitation balances evaporation) are related. Here we analyze dynamical and hydrological measures of the Southern Hemisphere edge of the tropics using simulations from the fifth Coupled Model Intercomparison Project (CMIP5) and four reanalysis data sets. In simulations with an abrupt quadrupling of atmospheric CO_2 concentrations, all models show a poleward expansion in both metrics. However, there is a large spread among models; the ratio of the hydrological to dynamical expansions varies from 0.6 to 1.4. We show that this model spread can be largely explained by differences in internal variability, which in turn is related to the mean state of models. Differences in mean states among reanalyses are similar to those of models, and so reanalyses do not help constrain uncertainty in model trends.

1. Introduction

Global climate models robustly predict that the Hadley circulation will expand poleward in response to increasing greenhouse gas concentrations (Frierson et al., 2007; Lu et al., 2007), most notably in the Southern Hemisphere (SH). As well as this large-scale circulation change, models also project significant changes to the global hydrological cycle, including a drying and poleward migration of the subtropical dry zones (Collins et al., 2013; Neelin et al., 2006). Several studies have proposed that much of the hydrological response to warming can be explained by thermodynamics, through an enhancement of moisture flux divergence resulting from a Clausius-Clapeyron increase in water vapor concentrations (Chou & Neelin, 2004; Held & Soden, 2006; Mitchell et al., 1987). However, recent work has argued that hydrological changes may also be caused by the direct radiative effect of increasing CO_2 (Bony et al., 2013; He & Soden, 2017) as well as by changes in atmospheric dynamics, in particular, the poleward expansion of the Hadley circulation (Previdi & Liepert, 2007; Seager et al., 2010; Scheff & Frierson, 2012a, 2012b). The relative roles of these dynamic and thermodynamic processes in governing future hydrological changes remain an area of significant uncertainty.

Previous studies have investigated the relationship between the edge of the Hadley cell and the edge of the subtropical dry zones, but these studies have reached seemingly opposing conclusions. Solomon et al. (2016) showed there to be a strong positive interannual correlation between these two metrics in reanalysis data, except during austral winter. On the other hand, Davis and Birner (2017) analyzed a different set of reanalyses and argued that there is no significant interannual relationship. Modeling studies that have investigated shifts of the Hadley cell and subtropical dry zones under greenhouse warming scenarios have also reached somewhat conflicting conclusions. A number of studies have reported a strong, approximately one-to-one, relationship between the magnitude of the shift of the Hadley cell and that of the subtropical dry zones (Lu et al., 2007; Polvani et al., 2011; Quan et al., 2014). However, Solomon et al. (2016) showed, using simulations of the Community Earth System Model (CESM), that the projected poleward shift of the Hadley cell is about twice that of the subtropical dry zones as the climate warms. It is unclear to what extent these contrasting results arise from differences in the models or reanalyses studied, differences in the forcing scenarios, or differences in the dynamical and hydrological metrics used.

Here we aim to address these issues by investigating the relationship between the Hadley circulation and the extent of the subtropical dry zones in both reanalysis data and climate model simulations. We limit our study to the SH since there the circulation is better approximated by zonal means (Schmidt & Grise, 2017) and the effects of land-sea temperature contrast, which may significantly affect the hydrological and dynamical responses to increasing CO_2 (He & Soden, 2017; Shaw & Voigt, 2015), are less important. We aim to address the following questions: (1) How consistent is the interannual relationship between the Hadley cell edge and the subtropical dry zones among climate models and reanalyses? (2) How robust is the relative response of the Hadley cell and subtropical dry zones to greenhouse warming among climate models? (3) Can biases in model climatologies (i.e., in their mean state or variability) explain differences in, and therefore be used to constrain, their greenhouse warming response? The climate model simulations, reanalysis data, and metrics studied are discussed in the following section. Section 3.1 addresses internal variability (question 1), section 3.2 addresses the response to greenhouse warming (questions 2 and 3), and conclusions are presented in section 4.

2. Data and Methodology

In our analysis we use simulations from 23 coupled climate models from the Coupled Model Intercomparison Project phase 5 (Taylor et al., 2012). CMIP5 data are freely available from the Program for Climate Model Diagnosis and Intercomparison (PCDMI) at Lawrence Livermore National Laboratory and from the UK Centre for Environmental Data Analysis. The 23 models selected here are the same as those used by Grise and Polvani (2016), and are listed in Figure 3. For each model, we examine two different forcing scenarios: (1) Preindustrial control simulations (>200 years of unforced variability), (2) abrupt $4 \times CO_2$ simulations (150 year simulations in which atmospheric CO_2 concentrations are abruptly quadrupled at the start of the simulation).

In addition, we analyze four contemporary "third-generation" reanalyses, using data from the post-1979 satellite era. Specifically we use data from the National Centers for Environmental Prediction (NCEP) Climate Forecast System Reanalysis (CFSR; Saha et al., 2010) (data from 1979 to 2010), the European Centre for Medium-Range Weather Forecasts Interim Reanalysis (ERA-Interim; Dee et al., 2011) (data from 1979 to 2016), the Japanese Meteorological Agency 55 year reanalysis (JRA-55; Kobayashi et al., 2015) (data from 1979 to 2013), and the National Aeronautics and Space Administration (NASA) Modern Era Retrospective Analysis for Research and Applications 2 (MERRA2; Gelaro et al., 2017) (data from 1980 to 2016). There are many differences in the construction of these reanalysis data sets, and a detailed description is given by Fujiwara et al. (2017). One of the more significant differences is the fact that CFSR is the only reanalysis with a coupled ocean, while the others use prescribed sea surface temperatures. Also of relevance for the following analysis is the fact that, unlike other reanalyses, MERRA-2 enforces a consistency between global evaporation, precipitation, and changes in atmospheric total water mass storage (Bosilovich et al., 2017).

For both model and reanalysis data, we calculate the following two zonal mean metrics:

1. *Poleward boundary of the Hadley circulation* ($\phi_{\Psi_{500}=0}$): The latitude at which the zonal mean meridional mass stream function at 500 hPa, Ψ_{500}, crosses zero, indicating the boundary between the thermally direct overturning circulation in the tropics and the thermally indirect overturning circulation in midlatitudes.
2. *Poleward edge of the subtropical dry zone* ($\phi_{P-E=0}$): The latitude at which zonal mean precipitation, P, balances evaporation, E (i.e., $P - E = 0$), indicating the transition from net evaporation in the subtropics to net precipitation in midlatitudes.

Following Grise and Polvani (2016), both metrics are first estimated using each model's native horizontal resolution, then a linear function is fit to the model data points surrounding this estimate, and then this function is used to refine the metric to 0.01° resolution. A similar linear interpolation technique is also applied to reanalysis data, following Davis and Rosenlof (2012). Annual or seasonal mean values of the $\phi_{\Psi_{500}=0}$ and $\phi_{P-E=0}$ metrics are computed from the relevant annual or seasonal mean fields, rather than by averaging monthly mean values of the metrics. We find this distinction to be somewhat important; for instance, the correlation of reanalysis annual mean $\phi_{\Psi_{500}=0}$ calculated from annual mean fields with that calculated from monthly mean values ranges from 0.97 (JRA-55) to just 0.54 (MERRA2). This choice of using annual or seasonal mean fields is consistent with Solomon et al. (2016), but differs from Davis and Rosenlof (2012) and Davis and Birner (2017) who use averages of monthly mean values.

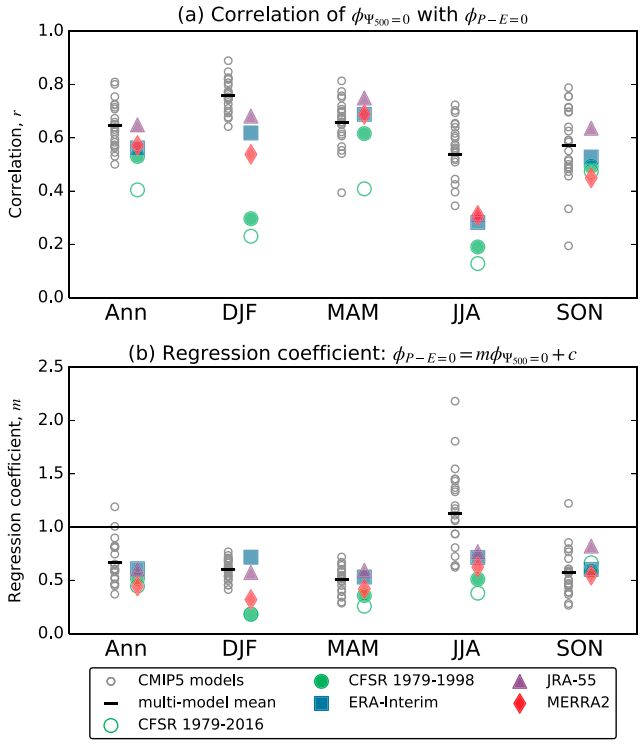

Figure 1. (a) Correlation coefficient, r, of annual and seasonal means of $\phi_{P-E=0}$ with $\phi_{\Psi_{500}=0}$ in 23 CMIP5 preindustrial control simulations and four reanalysis data sets. (b) As in Figure 1a but for the regression coefficient, m, calculated by a least squares fit of a linear relationship of the form $\phi_{P-E=0} = m\phi_{\Psi_{500}=0} + c$.

3. Results

3.1. Internal Variability

We begin by examining the interannual relationship between $\phi_{\Psi_{500}=0}$ and $\phi_{P-E=0}$ in the 23 CMIP5 model preindustrial control simulations and four reanalysis data sets. We calculate both the interannual correlation, r (Figure 1a), of annual and seasonal mean values of $\phi_{\Psi_{500}=0}$ and $\phi_{P-E=0}$, as well as the regression coefficient, m (Figure 1b), calculated by a linear least squares fit of a relationship of the form $\phi_{P-E=0} = m\phi_{\Psi_{500}=0} + c$. Therefore, m is the expected shift of $\phi_{P-E=0}$ for a 1° shift in $\phi_{\Psi_{500}=0}$. In order to isolate the interannual variability in these metrics, reanalysis values are shown after removing a linear trend. Relative to the other reanalyses, CFSR displays a significantly weaker correlation between $\phi_{\Psi_{500}=0}$ and $\phi_{P-E=0}$ for the annual mean and each season except austral spring (SON). This weaker relationship in CFSR appears to arise predominantly from its hydrological $\phi_{P-E=0}$ metric; the average correlation of CFSR annual mean $\phi_{P-E=0}$ with the other three reanalyses is just 0.6, while the CFSR $\phi_{\Psi_{500}=0}$ is in better agreement with the other reanalyses, with a mean correlation of 0.8 (Figure S1 in the supporting information). Furthermore, the discrepancy between $\phi_{P-E=0}$ in CFSR and in other reanalyses becomes particularly prominent after 1998 (Figure S2). Previous studies have attributed different drivers of tropical expansion during the period from 1979 to the late 1990s, when the ozone hole was expanding and global mean surface temperature increasing, and the "hiatus" period from the late 1990s, when temperature rise slowed and the ozone hole remained roughly constant (Adam et al., 2014; Waugh et al., 2015). However, we find that changes in the variability or trends of the tropical edge metrics between these two periods are not consistent among reanalyses, as may be expected if they were the result of common drivers. Rather, we propose that the jump in CFSR $\phi_{P-E=0}$ after 1998 is the result of the introduction of advanced microwave sounding unit (AMSU) radiances into the assimilation at this time. Indeed, a sharp increase in CFSR global mean water mass imbalance around 1998 was documented and attributed to AMSU assimilation by Saha et al. (2010). For this reason, for the remainder of this study we use CFSR data from 1979 to 1998 only (Figure 1, solid green circles), which have values of r in better agreement with the other reanalyses than the full 1979–2016 period (Figure 1, open green circles).

Interestingly, CFSR was included in the analysis of Davis and Birner (2017), who proposed that there is not a significant interannual correlation between $\phi_{\Psi_{500}=0}$ and $\phi_{P-E=0}$, but it was not included by Solomon et al. (2016), who showed there to be a strong correlation. Hence we propose that the anomalously weak relationship seen in CFSR is a major cause of these apparently conflicting conclusions (differences in the time averaging used in these two studies, as noted in section 2, also contribute to this discrepancy, though to a much lesser extent; N. Davis, personal communication, 2017).

All models show a statistically significant correlation ($p < 0.01$) between $\phi_{\Psi_{500}=0}$ and $\phi_{P-E=0}$ both for the annual mean and for each season, with the exception of the FGOALS-s2 model for JJA. There is, however, a large spread in the correlation among models; for the annual mean, correlations range from 0.44 (CNRM-CM5) to 0.82 (IPSL-CM5A-LR). Models also show a seasonal cycle in the relationship, with the correlation between $\phi_{\Psi_{500}=0}$ and $\phi_{P-E=0}$ being greatest in austral summer and lowest in winter, consistent with Polvani et al. (2011) and Solomon et al. (2016). In comparison, reanalyses show a slightly delayed seasonal cycle, with the highest correlation in austral autumn. Overall, there is good agreement between the interannual variability of reanalyses and models for annual mean values, since all reanalyses fall within the model spread; however, this agreement does not hold for seasonal values.

3.2. Response to CO_2 Quadrupling

We next examine the simulated annual mean response of $\phi_{P-E=0}$ and $\phi_{\Psi_{500}=0}$ to an abrupt quadrupling of CO_2 concentrations in the 23 CMIP5 models. All models show a poleward shift in both metrics (Figure 2a), but there is a large range in their magnitudes, from about 0.5° to 3° latitude. The majority of this spread

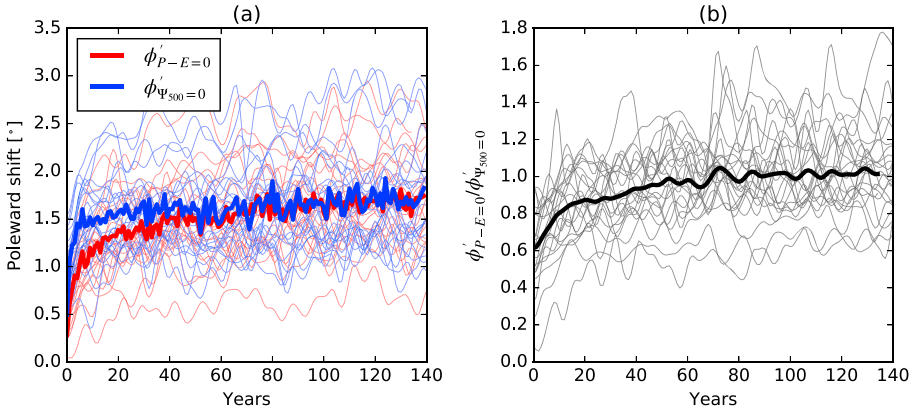

Figure 2. (a) Annual mean $\phi'_{P-E=0}$ and $\phi'_{\Psi_{500}=0}$ following an abrupt quadrupling of CO_2 concentrations at year 0 in 23 CMIP5 models. (b) Ratio of annual mean $\phi'_{P-E=0}/\phi'_{\Psi_{500}=0}$. Values are smoothed with a decadal running mean. Thin lines show the 23 individual CMIP5 models and thick lines show the multimodel mean.

has been attributed to differences in models' global mean surface temperature response, specifically their equilibrium climate sensitivity (Davis et al., 2016; Grise & Polvani, 2016); models that have a larger temperature rise simulate a larger poleward shift of both $\phi_{P-E=0}$ and $\phi_{\Psi_{500}=0}$. However, Grise and Polvani (2017) showed that these two metrics respond to increasing CO_2 on different time scales. This is seen here in that $\phi'_{P-E=0}$ is on average smaller than $\phi'_{\Psi_{500}=0}$ over the first 50 years following CO_2 quadrupling (here primes denote anomalies from the climatology of the control simulation), and is a result of $\phi'_{P-E=0}$ approximately tracking global mean surface temperature rise, while $\phi'_{\Psi_{500}=0}$ responds more rapidly as the result of the direct radiative effects of increased CO_2 (Grise & Polvani, 2017) or the fast adjustment of sea surface temperature patterns (Ceppi et al., 2017). The difference in time scales is further highlighted in Figure 2b, which shows that the ratio $\phi'_{P-E=0}/\phi'_{\Psi_{500}=0}$ increases over the first 50 years before equilibrating near a value of 1. However, models also show a large spread in this ratio; some models have $\phi'_{P-E=0}$ almost 50% larger than $\phi'_{\Psi_{500}=0}$, while others show $\phi'_{\Psi_{500}=0}$ almost 50% larger than $\phi'_{P-E=0}$. It is this large spread in the *relative* rates of expansion of $\phi_{P-E=0}$ and $\phi_{\Psi_{500}=0}$ that has, to our knowledge, not yet been investigated, and will be the focus of the following analysis.

Our hypothesis is that the model spread in the relative shifts of $\phi_{P-E=0}$ and $\phi_{\Psi_{500}=0}$ in response to increasing CO_2 can be explained through differences in the models' internal variability. This is examined in Figure 3, which shows the relationship between the models' annual mean interannual regression coefficients, m (as shown in Figure 1b), and the ratio of the responses to abrupt CO_2 quadrupling, $\phi'_{P-E=0}/\phi'_{\Psi_{500}=0}$. Importantly, the internal variability, m, can be seen to explain a large fraction of the intermodel variance in the relative responses (about 60% of the variance over the first 20 years of the simulations and about 40% from years 50 to 150). Note that the MPI-ESM-P, MPI-ESM-LR, and FGOALS-s2 models have been excluded from the correlations shown in Figure 3 because neither MPI-ESM-P or MPI-ESM-LR show the $\phi'_{P-E=0}/\phi'_{\Psi_{500}=0}$ ratio increasing with time as shown by all other models, and since FGOALS-s2 is a clear outlier from other models. However, the correlations remain significant if these models are included ($r = 0.63$ for years 0–20, and $r = 0.37$ for years 50–150). The interannual correlation coefficient, r, is also correlated with the $\phi'_{P-E=0}/\phi'_{\Psi_{500}=0}$ ratio, but this relationship is weaker than that with m ($r = 0.41$ for years 0–20, and $r = 0.46$ for years 50–150). Hence, we propose that m, rather than r, is the more important measure of interannual variability for determining the response to increasing CO_2.

All models except FGOALS-s2 have $m < 1$, indicating that for the models' internal variability, a given shift of $\phi_{\Psi_{500}=0}$ is accompanied by a smaller shift in $\phi_{P-E=0}$. The initial response to increasing CO_2 is closely related to this interannual variability (Figure 3a), as seen by the fact that almost all models also have $\phi'_{P-E=0}/\phi'_{\Psi_{500}=0} < 1$ and the best fit line (dashed) lies close to the 1:1 line (solid), with a small vertical offset. Over time, this offset grows such that for years 50–150 of the simulations, about half of the models have $\phi'_{P-E=0}/\phi'_{\Psi_{500}=0} > 1$ (Figure 3b). This again illustrates the different time scales of the responses of $\phi_{P-E=0}$ and $\phi_{\Psi_{500}=0}$ to increasing CO_2. Despite this time dependence of $\phi'_{P-E=0}/\phi'_{\Psi_{500}=0}$, at all times the internal variability m explains a large fraction of the spread between models. This is further highlighted in Figure S3, which shows best fit lines as in Figure 3 but for the responses averaged over consecutive 20 year periods (again excluding the MPI-ESM-P, MPI-ESM-LR, and FGOALS-s2 models). Here the ratio of $\phi'_{P-E=0}/\phi'_{\Psi_{500}=0}$ can again be seen to increase over time

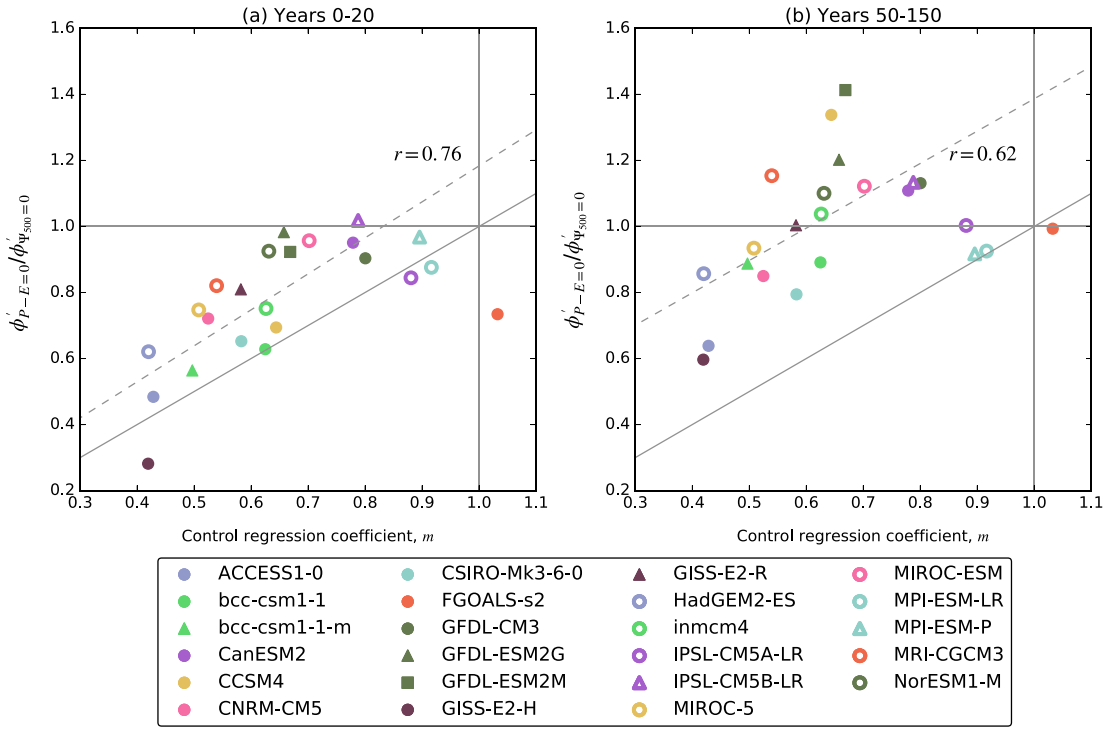

Figure 3. Ratio of annual mean shift of $\phi_{P-E=0}$ to annual mean shift of $\phi_{\Psi_{500}=0}$, for (a) years 0–20 and (b) years 50–150 of the 4 × CO_2 experiment in 23 CMIP5 models. Values are plotted against the regression coefficient, *m*, calculated from the CMIP5 control simulations. A linear best fit is shown (dashed), along with the correlation coefficient, *r*, and a 1:1 line (solid). The MPI-ESM-P, MPI-ESM-LR, and FGOALS-s2 models are outliers and have been excluded from the linear fit.

and stabilize after about 60 years. The best fit lines are approximately parallel, and the regression coefficients for each time period (see legend) are all statistically significantly greater than zero ($p < 0.05$, according to a two-tailed *t* test).

Having shown that the models' internal variability is crucial in determining their relative responses of $\phi'_{P-E=0}$ and $\phi'_{\Psi_{500}=0}$ to greenhouse warming, we next study possible causes for these differences in internal variability. A candidate for such a cause is intermodel differences in their climatological mean state. The relationship between the models' mean distance between the Hadley cell edge and subtropical dry zone edge, $\langle\phi_{\Psi_{500}=0}\rangle - \langle\phi_{P-E=0}\rangle$ (here angle brackets denote the climatological mean), and their interannual relationship *m* is shown in Figure 4a (circles). The value of $\langle\phi_{\Psi_{500}=0}\rangle - \langle\phi_{P-E=0}\rangle$ varies greatly among models (range of about 4° latitude) and is statistically significantly correlated with *m*. While the correlation in Figure 4a shows that other factors must also be responsible for generating the intermodel variance in *m* ($\langle\phi_{\Psi_{500}=0}\rangle - \langle\phi_{P-E=0}\rangle$ explains just 22% of the intermodel variance), the idea that models in which $\langle\phi_{\Psi_{500}=0}\rangle$ and $\langle\phi_{P-E=0}\rangle$ are closer show a nearer to one-to-one interannual relationship is physically intuitive. For instance, if the response of $P - E$ to a given shift of $\phi_{\Psi_{500}=0}$ were localized near $\phi_{\Psi_{500}=0}$ then one would expect a larger impact on $\phi_{P-E=0}$ if $\phi_{P-E=0}$ is close to $\phi_{\Psi_{500}=0}$, but little impact if the two are far apart. However, we also find that the magnitude of the $P - E$ response to a given $\phi_{\Psi_{500}=0}$ shift varies substantially among models and is generally smaller for larger values of $\langle\phi_{\Psi_{500}=0}\rangle - \langle\phi_{P-E=0}\rangle$ (not shown). This also goes some way to explaining the correlation shown in Figure 4a, but the physical mechanism behind this is unclear and a topic for future investigation.

Figures 4b and 4c show that $\langle\phi_{\Psi_{500}=0}\rangle - \langle\phi_{P-E=0}\rangle$ is also statistically significantly correlated with both the initial (years 0–20) and long-term (years 50–150) responses of $\phi'_{P-E=0}/\phi'_{\Psi_{500}=0}$ to abrupt CO_2 quadrupling. This relationship would be expected given the relationship between *m* and $\phi'_{P-E=0}/\phi'_{\Psi_{500}=0}$ shown in Figure 3. Note also that individually, $\langle\phi_{P-E=0}\rangle$ is significantly correlated with *m*, though its correlation with $\phi'_{P-E=0}/\phi'_{\Psi_{500}=0}$ not statistically significant for either time period, and $\langle\phi_{\Psi_{500}=0}\rangle$ is not correlated with either *m* or $\phi'_{P-E=0}/\phi'_{\Psi_{500}=0}$ (Figure S4). Hence, $\langle\phi_{\Psi_{500}=0}\rangle - \langle\phi_{P-E=0}\rangle$ appears to be the most important climatological mean metric.

We have established that there are significant differences in the interannual relationship of $\phi_{P-E=0}$ and $\phi_{\Psi_{500}=0}$ among reanalyses (Figure 1). However, it may be possible to use the climatological mean state from reanalyses,

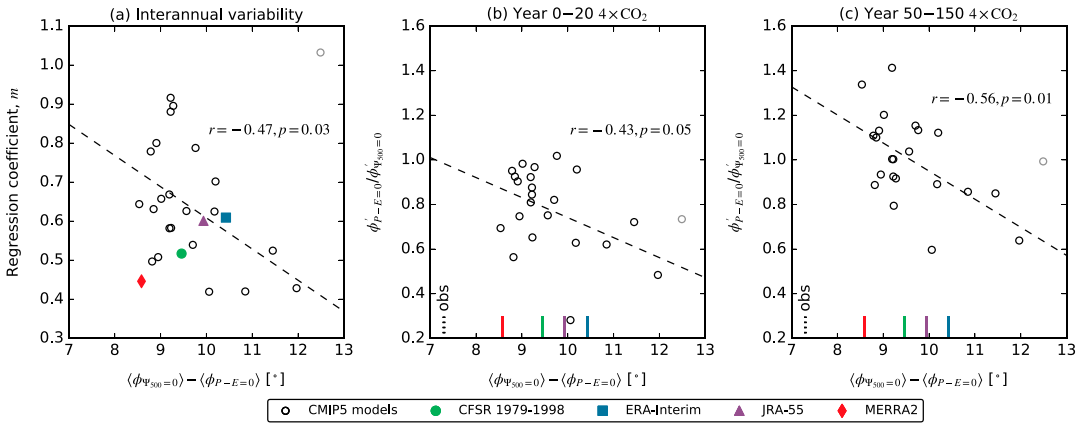

Figure 4. Relationship between the climatological mean distance between the Hadley cell edge and the edge of the subtropical dry zones, $\langle\phi_{\Psi_{500}=0}\rangle - \langle\phi_{P-E=0}\rangle$, and (a) the regression coefficient, m for interannual variability in 23 CMIP5 models and five reanalyses, (b) the initial response (years 0–20 average) of $\phi'_{P-E=0}/\phi'_{\Psi_{500}=0}$ to an abrupt quadrupling of CO_2, and (c) the long-term response (years 50–150 average). Correlation coefficients, r, for the relationship among models, are shown in each plot along with the p value for the null hypothesis that is $r = 0$ following a two-tailed t test. Best fit lines are also shown (dashed). Colored tick marks in Figures 4b and 4c indicate the values of reanalysis climatological means, and the dashed tick mark shows an observational estimate. The FGOALS-s2 model (shown in gray) is not included in the correlations.

along with the model-derived relationships shown in Figure 4 to constrain the projected response to increased CO_2. Figure 4a also includes values derived from the four reanalysis data sets. The reanalysis values of $\langle\phi_{\Psi_{500}=0}\rangle - \langle\phi_{P-E=0}\rangle$ span about 2° latitude, a large fraction of the intermodel spread. Note that the differences among reanalyses are consistent throughout the 1979–2009 period and are not a result of different trends among reanalyses or internal variability (Figure S2). The largest contributor to this spread comes from $\langle\phi_{P-E=0}\rangle$ rather than $\langle\phi_{\Psi_{500}=0}\rangle$, for which reanalyses are in much better agreement.

Motivated by this uncertainty, we also calculate an independent estimate of $\phi_{P-E=0}$ following Allen et al. (2014), using precipitation data from the Global Precipitation Climatology Project (GPCP; Adler et al., 2003) and evaporation data from the Woods Hole Oceanographic Institution (WHOI) Objectively Analyzed air-sea Flux (OAFlux) project (Yu & Weller, 2007). The WHOI OAFlux data are only available over the global oceans, so does not include evaporation from land; however, there is little land area near $\phi_{P-E=0}$ in the SH, so this bias should have a relatively small effect. This method gives a value of $\langle\phi_{P-E=0}\rangle$ of 39°S (time series shown in Figure S2), which is equatorward of all four reanalyses but closest to CFSR. However, CFSR has the lowest interannual correlation with the observationally derived $\phi_{P-E=0}$ estimate (0.4), while the other three reanalyses each have a correlation of 0.7. It is therefore not possible to straightforwardly conclude which of the reanalyses is in best agreement with this observational estimate. An estimate of $\langle\phi_{\Psi_{500}=0}\rangle - \langle\phi_{P-E=0}\rangle$ which uses the observational value of $\langle\phi_{P-E=0}\rangle$ and the multireanalysis mean of $\langle\phi_{\Psi_{500}=0}\rangle$ is also indicated in Figures 4b and 4c (labeled "obs"). This estimate is lower than any reanalysis or model value, and using the model-derived relaltionship between the mean state and response to CO_2 increases would tend to favor a larger value of $\phi'_{P-E=0}/\phi'_{\Psi_{500}=0}$. Overall, however, the large spread between reanalyses and observational estimates means that these do not provide a strong constraint on the models' internal variability or CO_2-induced trends.

4. Conclusions and Discussion

In this study we have focused on the relationship between the SH Hadley cell edge, $\phi_{\Psi_{500}=0}$, and the subtropical dry zone edge, $\phi_{P-E=0}$, as well as climate model projections of their *relative* rates of expansion under increased CO_2 concentrations. In other words, we have asked how much will the subtropical dry zones shift for a given shift in the Hadley cell? Our main findings are as follows:

1. There is a large spread in both the climatology and interannual variability of $\phi_{\Psi_{500}=0}$ and $\phi_{P-E=0}$ among reanalyses. These differences are largely responsible for the conflicting conclusions of Solomon et al. (2016) and Davis and Birner (2017), who studied slightly different sets of reanalyses.
2. Models show a large spread in the relative rates of poleward expansion of $\phi_{\Psi_{500}=0}$ and $\phi_{P-E=0}$ under increasing CO_2 concentrations. Some models have the shift in $\phi_{P-E=0}$ almost 50% larger than $\phi_{\Psi_{500}=0}$, while others

project a $\phi_{\Psi_{500}=0}$ shift almost 50% larger than $\phi_{P-E=0}$. As shown by Grise and Polvani (2017), $\phi_{P-E=0}$ is seen to shift on a slower time scale than $\phi_{\Psi_{500}=0}$ in almost every model.

3. The diversity of responses among models can be largely explained by the differences in their internal variability. Models with a higher ratio of $\phi_{P-E=0}/\phi_{\Psi_{500}=0}$ on interannual time scales also have a higher ratio under CO_2-forced changes.
4. Differences in internal variability are, in turn, related to the mean state of models. Models in which the mean value of $\phi_{P-E=0}$ is further equatorward and therefore closer to $\phi_{\Psi_{500}=0}$ show a nearer to one-to-one interannual relationship between the two, and hence project larger $\phi_{P-E=0}$ changes relative to $\phi_{\Psi_{500}=0}$ as the climate warms.

Solomon et al. (2016) showed that the expected shift of $\phi_{\Psi_{500}=0}$ is approximately twice that of $\phi_{P-E=0}$ under greenhouse gas increases using the CESM model. We can now put that result into wider context, with a greatly expanded ensemble of climate models. The majority of models show that the short-term response to increased CO_2 concentrations gives a larger $\phi_{\Psi_{500}=0}$ change than $\phi_{P-E=0}$ (Figure 3a), although there is a large spread among models with several showing almost equal shifts. However, over the longer term, about half of models show $\phi'_{\Psi_{500}=0} > \phi'_{P-E=0}$ and half show $\phi'_{P-E=0} > \phi'_{\Psi_{500}=0}$ (Figure 3b). Given this model diversity, we cannot place confidence in the result of Solomon et al. (2016) that the expected shift of the subtropical dry zones is less than that of the Hadley cell; indeed the result appears to be both time scale and model dependent. Furthermore, reanalysis or observational estimates do not significantly reduce this uncertainty. While the $4\times CO_2$ simulations analyzed here are highly idealized, the different time scales for the responses of $\phi_{\Psi_{500}=0}$ and $\phi_{P-E=0}$ can also be seen in simulations with more realistic, steady increases in CO_2 concentrations (Grise & Polvani, 2017).

The large differences among reanalyses in their climatological mean values of $\phi_{P-E=0}$ is perhaps not surprising given that global precipitation and evaporation are poorly constrained by observations, so that the underlying physical model used for the reanalysis plays a significant role in determining these values. Nonetheless, we have shown here that relative rates of the dynamical and hydrological expansion of the tropics are related to mean state and interannual variability of the atmosphere in climate models. As observational estimates of the mean state and variability improve in the future this relationship may provide an ever more useful tool to constrain climate model projections.

Acknowledgments
We thank two anonymous reviewers and Nick Davis for helpful comments and discussion of this work. The CMIP5 data used in this study are freely available through the Earth System Grid Federation (https://esgf-node.llnl.gov), and the metrics derived from this data are available from the authors on request. We acknowledge the World Climate Research Programme's Working Group on Coupled Modelling, which is responsible for CMIP, and we thank the climate modeling groups (listed in Figure 3) for producing and making available their model output. W. J. M. S. and D. W. W are partially supported by two awards (FESD-1338814 and AGS-1403676) from the U.S. National Science Foundation (NSF). K. M. G. is supported in part by NSF award AGS-1522829.

References

Adam, O., Schneider, T., & Harnik, N. (2014). Role of changes in mean temperatures versus temperature gradients in the recent widening of the Hadley circulation. *Journal of Climate*, *27*, 7450–7461. https://doi.org/10.1175/JCLI-D-14-00140.1

Adler, R. F., Huffman, G. J., Chang, A., Ferraro, R., Xie, P.-P., Janowiak, J., … Nelkin, E. (2003). The version-2 global precipitation climatology project (GPCP) monthly precipitation analysis (1979–present). *Journal of Hydrometeorology*, *4*, 1147–1167. https://doi.org/10.1175/1525-7541(2003)004<1147:TVGPCP>2.0.CO;2

Allen, R. J., Norris, J. R., & Kovilakam, M. (2014). Influence of anthropogenic aerosols and the Pacific Decadal Oscillation on tropical belt width. *Nature Geoscience*, *7*, 270–274. https://doi.org/10.1038/ngeo2091

Bony, S., Bellon, G., Klocke, D., Sherwood, S., Fermepin, S., & Denvil, S. (2013). Robust direct effect of carbon dioxide on tropical circulation and regional precipitation. *Nature Geoscience*, *6*, 447–451. https://doi.org/10.1038/ngeo1799

Bosilovich, M. G., Robertson, F. R., Takacs, L., Molod, A., & Mocko, D. (2017). Atmospheric water balance and variability in the MERRA-2 reanalysis. *Journal of Climate*, *30*, 1177–1196. https://doi.org/10.1175/JCLI-D-16-0338.1

Ceppi, P., Zappa, G., Shepherd, T. G., & Gregory, J. M. (2017). Fast and slow components of the extratropical atmospheric circulation response to CO_2 forcing. *Journal of Climate*. https://doi.org/10.1175/JCLI-D-17-0323.1

Chou, C., & Neelin, J. D. (2004). Mechanisms of global warming impacts on regional tropical precipitation. *Journal of Climate*, *17*, 2688–2701.

Collins, M., Knutti, R., Arblaster, J., Dufresne, J.-L., Fichefet, T., Friedlingstein, P., … Wehner, M. (2013). *Long-term climate change: Projections, commitments and irreversibility* (chap. 12, pp. 1029–1136). Cambridge, UK and New York: Cambridge University Press. https://doi.org/10.1017/CBO9781107415324.024

Davis, N., & Birner, T. (2017). On the discrepancies in tropical belt expansion between reanalyses and climate models and among tropical belt width metrics. *Journal of Climate*, *30*, 1211–1231.

Davis, N. A., Seidel, D. J., Birner, T., Davis, S. M., & Tilmes, S. (2016). Changes in the width of the tropical belt due to simple radiative forcing changes in the GeoMIP simulations. *Atmospheric Chemistry and Physics*, *16*, 10,083–10,095. https://doi.org/10.5194/acp-16-10083-2016

Davis, S. M., & Rosenlof, K. H. (2012). A multidiagnostic intercomparison of tropical-width time series using reanalyses and satellite observations. *Journal of Climate*, *25*, 1061–1078. https://doi.org/10.1175/JCLI-D-11-00127.1

Dee, D. P., Uppala, S. M., Simmons, A. J., Berrisford, P., Poli, P., Kobayashi, S., … Vitart, F. (2011). The ERA-Interim reanalysis: Configuration and performance of the data assimilation system. *Quarterly Journal of the Royal Meteorological Society*, *137*, 553–597. https://doi.org/10.1002/qj.828

Frierson, D. M. W., Lu, J., & Chen, G. (2007). Width of the Hadley cell in simple and comprehensive general circulation models. *Geophysical Research Letters*, *34*, L18804. https://doi.org/10.1029/2007GL031115

Fujiwara, M., Wright, J. S., Manney, G. L., Gray, L. J., Anstey, J., Birner, T., … Zou, C.-Z. (2017). Introduction to the SPARC Reanalysis Intercomparison Project (S-RIP) and overview of the reanalysis systems. *Atmospheric Chemistry and Physics*, *17*, 1417–1452. https://doi.org/10.5194/acp-17-1417-2017

Gelaro, R., McCarty, W., Suárez, M. J., Todling, R., Molod, A., Takacs, L., … Zhao, B. (2017). The Modern-Era Retrospective analysis for Research and Applications, version 2 (MERRA-2). *Journal of Climate*, *30*, 5419–5454. https://doi.org/10.1175/JCLI-D-16-0758.1

Grise, K. M., & Polvani, L. M. (2016). Is climate sensitivity related to dynamical sensitivity? *Journal of Geophysical Research*, *121*, 5159–5176. https://doi.org/10.1002/2015JD024687

Grise, K. M., & Polvani, L. M. (2017). Understanding the timescales of the tropospheric circulation response to abrupt CO_2 forcing in the Southern Hemisphere: Seasonality and the role of the stratosphere. *Journal of Climate*, *30*, 8497–8515. https://doi.org/10.1175/JCLI-D-16-0849.1

He, J., & Soden, B. J. (2017). A re-examination of the projected subtropical precipitation decline. *Nature Climate Change*, *7*, 53–57. https://doi.org/10.1038/nclimate3157

Held, I. M., & Soden, B. J. (2006). Robust responses of the hydrological cycle to global warming. *Journal of Climate*, *19*, 5686–5699. https://doi.org/10.1175/JCLI3990.1

Kobayashi, S., Ota, Y., Harada, Y., Ebita, A., Moriya, M., Onoda, H., … Takahashi, K. (2015). The JRA-55 reanalysis: General specifications and basic characteristics. *Journal of the Meteorological Society of Japan*, *93*, 5–48. https://doi.org/10.2151/jmsj.2015-001

Lu, J., Vecchi, G. A., & Reichler, T. (2007). Expansion of the Hadley cell under global warming. *Geophysical Research Letters*, *34*, L06805. https://doi.org/10.1029/2006GL028443

Mitchell, J. F. B., Wilson, C. A., & Cunnington, W. M. (1987). On CO_2 climate sensitivity and model dependence of results. *Quarterly Journal of the Royal Meteorological Society*, *113*, 293–322. https://doi.org/10.1002/qj.49711347517

Neelin, J. D., Münnich, M., Su, H., Meyerson, J. E., & Holloway, C. E. (2006). Tropical drying trends in global warming models and observations. *Proceedings of the National Academy of Sciences of the United States of America*, *103*, 6110–6115. https://doi.org/10.1073/pnas.0601798103

Polvani, L. M., Waugh, D. W., Correa, G. J. P., & Son, S.-W. (2011). Stratospheric ozone depletion: The main driver of twentieth-century atmospheric circulation changes in the Southern Hemisphere. *Journal of Climate*, *24*, 795–812. https://doi.org/10.1175/2010JCLI3772.1

Previdi, M., & Liepert, B. G. (2007). Annular modes and Hadley cell expansion under global warming. *Geophysical Research Letters*, *34*, L22701. https://doi.org/10.1029/2007GL031243

Quan, X.-W., Hoerling, M. P., Perlwitz, J., Diaz, H. F., & Xu, T. (2014). How fast are the tropics expanding? *Journal of Climate*, *27*, 1999–2013. https://doi.org/10.1175/JCLI-D-13-00287.1

Saha, S., Moorthi, S., Pan, H.-L., Wu, X., Wang, J., Nadiga, S., … Goldberg, M. (2010). The NCEP climate forecast system reanalysis. *Bulletin of the American Meteorological Society*, *91*, 1015–1057. https://doi.org/10.1175/2010BAMS3001.1

Scheff, J., & Frierson, D. (2012a). Twenty-first-century multimodel subtropical precipitation declines are mostly midlatitude shifts. *Journal of Climate*, *25*, 4330–4347. https://doi.org/10.1175/JCLI-D-11-00393.1

Scheff, J., & Frierson, D. M. W. (2012b). Robust future precipitation declines in CMIP5 largely reflect the poleward expansion of model subtropical dry zones. *Geophysical Research Letters*, *39*, L18704. https://doi.org/10.1029/2012GL052910

Schmidt, D. F., & Grise, K. M. (2017). The response of local precipitation and sea level pressure to Hadley cell expansion. *Geophysical Research Letters*, *44*, 10,573–10,582. https://doi.org/10.1002/2017GL075380

Seager, R., Naik, N., & Vecchi, G. A. (2010). Thermodynamic and dynamic mechanisms for large-scale changes in the hydrological cycle in response to global warming. *Journal of Climate*, *23*, 4651–4668. https://doi.org/10.1175/2010JCLI3655.1

Shaw, T. A., & Voigt, A. (2015). Tug of war on summertime circulation between radiative forcing and sea surface warming. *Nature Geoscience*, *8*, 560–566. https://doi.org/10.1038/ngeo2449

Solomon, A., Polvani, L. M., Waugh, D. W., & Davis, S. M. (2016). Contrasting upper and lower atmospheric metrics of tropical expansion in the Southern Hemisphere. *Geophysical Research Letters*, *43*, 10,496–10,503. https://doi.org/10.1002/2016GL070917

Taylor, K. E., Stouffer, R. J., & Meehl, G. A. (2012). An overview of CMIP5 and the experiment design. *Bulletin of the American Meteorological Society*, *93*, 485–498. https://doi.org/10.1175/BAMS-D-11-00094.1

Waugh, D. W., Garfinkel, C. I., & Polvani, L. M. (2015). Drivers of the recent tropical expansion in the Southern Hemisphere: Changing SSTs or ozone depletion? *Journal of Climate*, *28*, 6581–6586. https://doi.org/10.1175/JCLI-D-15-0138.1

Yu, L., & Weller, R. A. (2007). Objectively analyzed air-sea heat fluxes for the global ice-free oceans (1981–2005). *Bulletin of the American Meteorological Society*, *88*, 527–539. https://doi.org/10.1175/BAMS-88-4-527